Master Copy
6/00

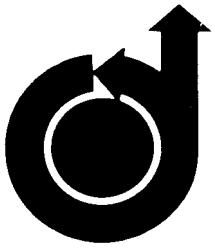

AIAA-81-2046

Sound Generated in a Cascade by Three-Dimensional Disturbances Convected in a Subsonic Flow

H. Atassi and G. Hamad
University of Notre Dame
Notre Dame, Indiana

7th AIAA AERO-ACOUSTICS CONFERENCE
Palo Alto, California/October 5-7,1981

SOUND GENERATED IN A CASCADE BY THREE-DIMENSIONAL DISTURBANCES CONVECTED IN A SUBSONIC FLOW†

H. Atassi* and G. Hamad**
Department of Aerospace and Mechanical Engineering
University of Notre Dame
Notre Dame, IN 46556

Abstract

Discrete tone sound generation in a subsonic fan subject to 3-D disturbances is investigated. The analytical model used treats the fan rotor and stator as linear cascades of thin airfoils in a rectangular duct subject to a 3-D gust for which a complete aerodynamic theory already exists. The sound pressure can then be cast as the sum of a finite number of discrete sound waves (modes) the magnitude of which depends on an unknown function satisfying a singular integral equation. Similarity rules are derived to reduce the problem to that of a 2-D gust. 3-D effects on the cut-off condition, the sound pressure, and the acoustic power are first investigated for each mode. The theory is then applied to noise generated by typical rotor-wake-defect and rotor-tip-vortex disturbances interacting with a stator.

Nomenclature

a	$A_{p,q} \sin\mu + B_{p,q} \cos\mu$
b	blade span
c	chord length
c_ℓ	distance between tip vortex and blade tip
c_o	speed of sound
d	interblade distance
d^+	$[(s^+)^2 + \beta_r^2 s^2]^{1/2}$
$f_o(\alpha)$	solution of Eq. (17)
i	$\sqrt{-1}$
$\vec{i}_2,\vec{j}_2,\vec{K}$	unit vectors in the x_2,y_2, and z directions
k_1	$\omega c/(2U_r)$
k_3	$\pi qc/(2b)$
n	integer specifying acoustic waves
p	acoustic pressure, Fourier expansion index in $\vec{j}_1$ direction
$\vec{q}$	disturbance velocity
q	Fourier expansion index in $\vec{K}$ direction
r_M	mean radius of fan
s	blade distance measured normal to chord
s_1	suction side velocity defect width
s_2	pressure side velocity defect width
s^+	stagger distance measured parallel to chord
t	time
v_1	unsteady velocity normal to blade
v_v	velocity distribution due to tip vortex
v_w	velocity distribution due to viscous wake
x,y,z	duct coordinates, x-axis in axial direction
x_2,y_z,z	cascade coordinates, x_2-axis parallel to blade
A	vortex intensity
$A_{p,q},B_{p,q}$	Fourier coefficients of 3-D disturbances
B	number of rotor blades
H	velocity defect amplitude
$\vec{I}$	acoustic intensity
$\vec{I}_1,\vec{J}_1,\vec{K}$	unit vectors in the X_1,Y_1,Z directions
K	$2k_1M_r/\beta_r^2$
K_q	$\pi qc/(\beta_r b)$
L	$\bar{L}/(\pi\rho_o c U_r a)$
$\bar{L}$	aerodynamic lift
M_o	U_o/c_o
M_r	U_r/c_o
P	defined by Eq. (7)
S	duct area
U_o	velocity of rotor
U_∞	incoming mean velocity
U_r	mean velocity relative to stator
V	defined by Eq. (8)
W	acoustic power
α_n	defined by Eq. (31)
β_r	$(1 - M_r^2)^{1/2}$
γ	$(\alpha^2 - \kappa^2)^{1/2}$
δ_n,θ_n,χ^+	defined by Eqs. (35)
ε	tip vortex width in span direction
κ	$(K^2 - K_q^2)^{1/2}$
μ	gust angle
ν	angle of incoming velocity with machine axis
ξ,η	Prandtl-Glauert coordinates
ρ	density
σ	interblade phase angle
ω	Ωp
Γ	defined by Eq. (20)
χ	stagger angle
Ω	angular velocity of rotor

Subscripts

n	mode number
p,q	Fourier expansion indices

Superscripts

+	upstream propagation
-	downstream propagation

I. Introduction

For aircraft turbofan engines operating at subsonic flow conditions, the noise spectrum consists of a number of discrete tones superimposed on a broad band spectrum. The discrete or pure tones are mainly distributed at integer multiples of the blade passing frequency of the fan. They constitute

† Research supported by a grant from NASA Lewis Research Center, No. NSG 3195.
* Professor of Aerospace and Mechanical Engineering, Member AIAA.
**Research Assistant, Student Member AIAA.

the most objectionable part of the noise spectrum [1].

Discrete tones may be generated by steady rotor blade forces in a similar fashion to the Gutin mechanism for propellers, or they may result from the interaction of flow nonuniformities with the fan rotor blades or guide vanes. However, in fan acoustics one has to consider simultaneously the mechanism generating the sound waves and their transmission through the duct. Tyler and Sofrin [2] have shown that at subsonic tip Mach number, the symmetrically distributed spinning modes of a single rotor are not likely to propagate in the duct, but rather will decay rapidly. This eliminates the steady aerodynamic loading of rotor blades as a source of noise. But when the rotor is operating in a spatially nonuniform flow due to inlet distortion or inlet turbulence some of the resulting modes will propagate along the duct. Similarly, when the rotor is operating in combination with stator vanes, many patterns are generated, some of which may be spinning above their critical Mach number. These high speed patterns will also propagate along the duct and radiate sound outside.

Hence, there are essentially two relevant noise generating mechanisms in subsonic fans, namely, inlet distortion and turbulence interacting with the rotor, and rotor-stator interaction. Both are governed by the same aerodynamic process: a row of blades swept by a spatially nonuniform but periodic flow.

Recent investigations of fan noise by Cumpsty and Lowrie [3], and Feiler and Merriman [4] have indicated that the rotor-stator interaction is the dominant source of pure tone noise for subsonic fans in flight. This interaction, first studied by Kemp and Sears [5], has been traditionally viewed as the interaction of the rotor blade wakes with the downstream vanes. However, in a recent review, Dittmar [6] has pointed out the importance of interaction of rotor blade tip vortices and velocity defects with the downstream stator vanes as a source of pure tone noise. Dittmar further suggested that rotor tip flow irregularities interacting with stator blades would produce noise of comparable strength to the more commonly studied rotor wake-stator interaction mechanism.

The objective of the present paper is to calculate the noise level and spectrum produced in response to every source of flow nonuniformities, and thus to establish the dominant noise generating mechanism of the fan. In subsonic fans, the type of flow nonuniformities superimposed on the mean flow is well illustrated by the flow behind a row of rotor blades. Figure (1) schematically shows the development of viscous wakes, the formation of tip and hub vortices, and the establishment of secondary flows. Detailed investigations of such flows have been carried out by Raj and Lakshminarayana [7] and Ravindrath and Lakshminarayana [8]. It is important to note the three-dimensional character of these flow irregularities. Their decay rate slows down as they move downstream and their magnitude as they interact with a subsequent stator row is usually small compared to the mean flow velocity. Hence they can be approximated by frozen small amplitude disturbances convected by the mean flow.

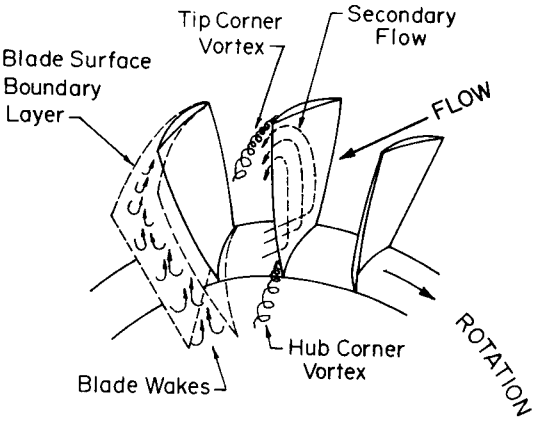

Fig. 1 Schematic Representation of Flow Behind a Rotor Blade Row.

In this paper, we study sound generation in a cascade of thin airfoils subject to three-dimensional vortical disturbances convected in a subsonic uniform flow. Essentially there are two approaches to this problem. One approach is to use Lighthill's analogy [9] to calculate the sound field. Goldstein et al. [10] used this method to calculate inlet flow distortion noise in a two-dimensional fan. Kobayashi and Groeneweg [11] carried out similar calculations for a three-dimensional fan and accounted for the effects of noncompact sources. This approach usually uses certain approximations regarding the fluctuating dipole distribution along the fan blades. The other method is to directly solve the inviscid flow equations subject to the boundary conditions on the fan blades and the duct walls. This method yields the sound field as the far field solution. The theory is greatly simplified by assuming the two-dimensional fan approximation; that is by unrolling the fan and replacing the annular duct by a rectangular duct. The periodicity condition of the annular duct is here accounted for by considering an infinite linear cascade of thin airfoils.

In the present analysis, we use the rectangular fan approximation and employ the direct method to calculate the sound propagating in the fan duct. As will be discussed below, a mathematical theory treating this problem already exists and has been applied to two-dimensional disturbances. The emphasis of this paper will hence be on calculating and analyzing the sound generated by three-dimensional vortical disturbances interacting with a linear cascade. It is convenient in the following to describe the interaction mechanism producing the sound as a rotor wake-stator interaction. The basic analysis and results essentially apply to stator wake-rotor interaction and to inlet distortion and turbulence interacting with a rotor. Any significant differences will be pointed out in the analysis.

II. Theoretical Formulation

The mathematical theory for a linear cascade of flat plate airfoils in subsonic flow was first developed for two-dimensional disturbances by Lane and Friedman [12]. The theory leads to a singular

integral equation for the pressure distribution along the airfoil surface. Using this theoretical framework, Kaji and Okazaki [13] and Whitehead [14] studied the sound generation in cascade and obtained expressions for the far field solution corresponding to the outgoing sound waves in the cascade. The theory was extended by Goldstein [1, ch.5] to account for three-dimensional disturbances. The present work follows very closely the theory developed by Goldstein, and the notation has been chosen so as to be largely identical with his. Details of the mathematical derivation will be found in Goldstein's book, only those necessary for undertaking the present work will be reproduced here.

We consider a stator cascade of flat plates of chord length c and span b at an angle χ to the axis of the machine as shown in Figure (2). The cascade

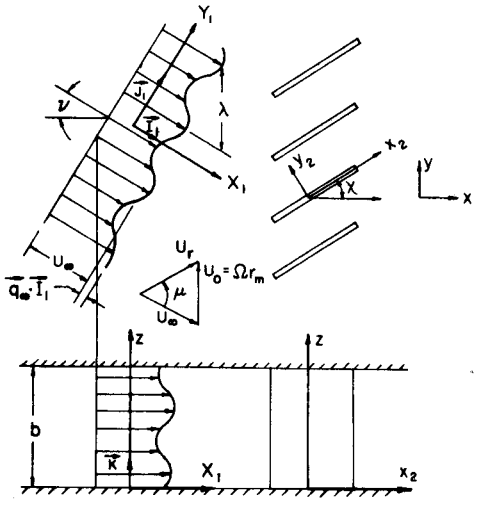

Fig. 2. Flow into Cascade.

is located between two infinite horizontal plates at distance b from each other. Upstream of this linear cascade, there is a rotor moving with a linear velocity $U_o = \Omega r_M$, where Ω is the angular velocity of the rotor and r_M is some mean radius of the fan. The mean flow behind the rotor has a velocity U_∞ at angle ν to the machine axis. Superimposed to U_∞ is a three-dimensional disturbance $\vec{q}_\infty$ which can be represented by a double Fourier series in the coordinates Y_1 and z. Applying the condition that $\vec{q}_\infty$ is solenoidal and expressing Y_1 in terms of the coordinates $x_2 - y_2$, we obtain the following expression

$$\vec{q}_\infty = \sum_{p,q} (\vec{I}_1 A_{p,q} + \vec{J}_1 B_{p,q}) \cos\left(\frac{\pi q z}{b}\right) - \vec{K} \frac{2ipb}{L_o q \cos\nu} B_{p,q} \sin\left(\frac{\pi q z}{b}\right) \times e^{ip\Omega[(x_2 + y_2 \cot\mu)/U_r - t]} , \quad (1)$$

where $\vec{I}_1, \vec{J}_1$ and $\vec{K}$ are the unit vectors in the X_1-Y_1, and z directions respectively; $A_{p,q}$ and $B_{p,q}$ are complex constants; the angles ν and μ are defined in Fig. (2); and $L_o = 2\pi r_M$.

The disturbance velocity can then be written

$$\vec{q} = \vec{q}_\infty + \vec{q}_1 \quad . \quad (2)$$

Assuming the flow to be isentropic and non-heat conducting the equations governing $\vec{q}_1$ and the disturbance pressure p are

$$\rho_o \frac{D_o}{Dt} \vec{q}_1 = - \nabla P \quad , \quad (3)$$

$$\frac{1}{\rho_o c_o^2} \frac{D_o P}{Dt} = - \nabla \vec{q} \quad , \quad (4)$$

where ρ_o represents the mean density of the air; c_o, the speed of sound and

$$\frac{D_o}{D_t} \equiv \frac{\partial}{\partial t} + U_r \frac{\partial}{\partial x_2} \quad .$$

If we consider only one Fourier component of (1), the boundary condition to be satisfied by $\vec{q}_1$ is

$$v_1 = - a \cos\left(\frac{\pi q z}{b}\right) e^{ip\Omega[(x_2 + m s \cot\mu)/U_r - t]} \quad , \quad (5)$$

$$\text{for } \frac{-c}{2} < x_2 - m s^+ < \frac{c}{2}, \quad y_2 = ms, \quad 0 < z < b \quad \Big\} \; m = 0, \pm 1, \pm 2 \ldots \quad (6)$$

where v_1 is the component of $\vec{q}_1$ along the y_2-axis, $a = -A_{p,q} \sin\mu + B_{p,q} \cos\mu$, s is the interblade gap measured normal to the chord, s^+ is the stagger distance measured parallel to the chord, and c is the chord length. The cascade parameters are shown in Figure (3).

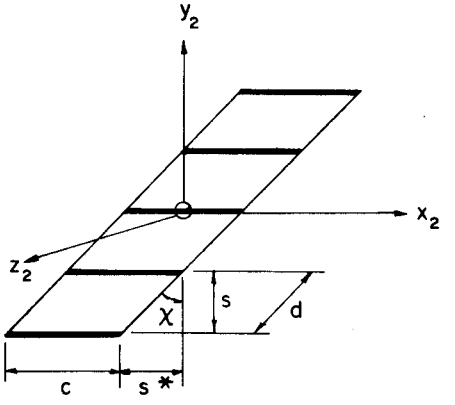

Fig. 3. Cascade Geometry.

Equation (5) suggests the use of the following new dependent variables.

$$p = -a\rho_o U_r P(x_2,y_2)e^{-i\omega t}\cos(\frac{\pi qz}{b}) \tag{7}$$

$$v_1 = -aV(x_2,y_2)e^{-i\omega t}\cos(\frac{\pi qz}{b}) \tag{8}$$

where $\omega = p\Omega = pU_o/r_M$. If one further introduces the Prandtl-Glauert coordinates $\xi = x_2/c$, and $\eta = \beta_r y_2/c$, as well as the new dependent variable

$$\Psi = P\, e^{iM_rK\xi} \tag{9}$$

it is possible to reduce Eqs. (3,4) to

$$\frac{\partial^2\Psi}{\partial\xi^2} + \frac{\partial^2\Psi}{\partial\eta^2} + (K^2 - K_q^2)\Psi = 0 \quad , \tag{10}$$

and

$$V = -\beta_r\, e^{i(\beta_r^2K\xi)/M_r}\int_{-\infty}^{\xi} e^{-i(K/M_r)\xi}\frac{d\Psi}{d\eta}\,d\xi \quad , \tag{11}$$

where

$$M_r \equiv \frac{U_r}{c_o} \quad , \tag{12}$$

$$\beta_r \equiv \sqrt{1 - M_r^2} \quad , \tag{13}$$

$$K \equiv \frac{\omega c}{c_o\beta_r^2} = 2k_1M_r/\beta_r^2 \quad , \tag{14}$$

$$K_q \equiv \frac{\pi q_c}{\beta_r b} = 2k_3/\beta_r \tag{15}$$

Note that $k_1 = \omega c/2U_r$ is the reduced frequency, and $k_3 = \pi qc/2b$ is the spanwise wave number. Hence the problem is reduced to solving (10) with the boundary conditions

$$\left.\begin{aligned} &\frac{d\Psi}{d\eta} = 0 \\ &V = e^{i(\beta_r^2\, K/M_r)(\xi + m\frac{s}{c}\cot\mu)} \end{aligned}\right\} \text{at} \begin{cases} -\frac{1}{2} < \xi - \frac{ms^+}{c} < \frac{1}{2} \\ \eta = \frac{ms}{c}\,\beta_r \end{cases} \tag{16}$$

A formal solution for V can be obtained in terms of a function $f_o(\alpha)$

$$V(\xi,\eta) = \frac{i\beta_r}{4}\int_{-\infty}^{\infty}\frac{M_r\, f_o(\alpha)\gamma(\alpha)e^{-i(\alpha + M_rK)\xi}}{K + M_r\,\alpha} \times\left[\frac{e^{-\eta\gamma} + (1/2)\Delta_+}{\sinh\frac{1}{2}\Delta_+} - \frac{e^{\eta\gamma} + (1/2)\Delta_-}{\sinh\frac{1}{2}\Delta_-}\right]d\alpha \tag{17}$$

for $0 \le \eta < \frac{s\beta_r}{c}$,

where

$$\Delta_{\pm}(\alpha) = i(\Gamma + \frac{\alpha s^+}{c}) \pm \frac{s\beta_r\gamma}{c} \quad , \tag{18}$$

$$\gamma(\alpha) = \sqrt{\alpha^2 - K^2 + K_q^2} \quad , \tag{19}$$

$$\Gamma \equiv \sigma + \frac{M_rKs^+}{c} = \frac{K}{M_r}(\frac{s^+}{c} + \frac{\beta_r^2 s}{c}\cot\mu) \quad . \tag{20}$$

σ is the so-called interblade phase angle. Applying conditions (16) at the surface of the blades yields the two simultaneous integral equations to be satisfied by $f_o(\alpha)$.

$$i\frac{\beta_r}{2}\int_{-\infty}^{+\infty}\frac{f_o(\alpha)}{\frac{K}{M_r} + \alpha}e^{-i(\alpha + \frac{K}{M_r})\xi}\gamma E(\alpha)\,d\alpha = 1, \quad \text{for } -\frac{1}{2} < \xi < \frac{1}{2} \tag{21}$$

and

$$f_o(\alpha) = \frac{1}{2\pi}\int_{-\frac{1}{2}}^{\frac{1}{2}}[P]\, e^{i(\alpha + M_rK)\xi}\,d\xi \quad . \tag{22}$$

that causes the pressure jump [P] to vanish at the trailing edge. Note that

$$E(\alpha) = \frac{\sinh\frac{s\beta_r\gamma}{c}}{\cosh\frac{s\beta_r\gamma}{c} - \cos(\Gamma + \frac{\alpha s^+}{c})} \tag{23}$$

accounts for cascade effects. For a single airfoil $E(\alpha) = 1$.

The solution of Eqs. (21) and (22) yields $f_o(\alpha)$ and the pressure jump [P] along the blade surface. The upstream and downstream acoustic pressure can then be obtained by considering the farfield upstream and downstream expressions of V given in (17) and using (7), (9) and (11).

It is important to note that because of the term $E(\alpha)$ in (21) there is a significant difference between the case of a cascade and that of a single airfoil. When the denominator of $E(\alpha)$ has a double root, $E(\alpha)$ has a non-integrable singularity and therefore $f_o(\alpha)$ and [P] vanish at the surface of the blade. Such a condition is known as the resonance condition and was first discussed for a cascade by Lane and Friedman [12]. In the present case the mathematical expression of the resonance condition can easily be given as

$$(\frac{c\Gamma_n}{d^+})^2 = K^2 - K_q^2 \quad , \tag{24}$$

where

$$\Gamma_n = \Gamma - 2n\pi \quad , \; n = 0, \pm 1, 2, \ldots, \tag{25}$$

$$d^+ = (s^{+2} + \beta_r^2 s^2)^{\frac{1}{2}} \quad .$$

The effects of resonance on the aerodynamics of the blades will be discussed in section (IV) and on the acoustic solution in section (V).

III. Similarity Rules for Airfoil and Cascades in Three-Dimensional Gusts

Similarity rules equivalent to those derived by Graham [15] for airfoils in oblique gusts can also be established for three-dimensional gusts acting upon airfoils and cascades. As we examine the present boundary-value problem defined by Eqs. (10) and (11) and conditions (16), we see that, as in Grahams case, it can be reduced to two simpler classes of problems depending whether $\theta = K/K_q$ is larger or smaller than one.

(a) Reduction to 2-D Gusts in Compressible Flows for $\theta > 1$.

For $K > K_q$, Eq. (10) is a Helmholtz equation similar to that governing the 2-D gust problem in compressible flow for which $K_q = o$ or $\theta = \infty$. Hence this class of flows can be reduced to the asymptotic case $\theta = \infty$ by the set of similarity rules:

$$\left.\begin{aligned}
&\text{(i)} \quad K_\infty = (K^2 - K_q^2)^{\frac{1}{2}} \quad , \\
&\text{(ii)} \quad K_{q_\infty} = 0 \quad , \\
&\text{(iii)} \quad M_{r_\infty} = M_r(1-1/\theta^2)^{\frac{1}{2}} \quad , \\
&\text{(iv)} \quad \left(\frac{s}{c}\right)_\infty = \left(\frac{s}{c}\right)\cdot \beta_r/(\beta_r)_\infty \quad , \\
&\text{(v)} \quad \left(\frac{s^+}{c}\right)_\infty = \left(\frac{s^+}{c}\right) \quad , \\
&\text{(vi)} \quad \cot\mu_\infty = [\beta_r/(\beta_r)_\infty]\cot\mu
\end{aligned}\right\} \qquad (26)$$

Equation (11) shows that $\Psi\beta_r$ is the same for the two flows, and therefore (9) gives

$$P(M,s,s^+,\mu,K,K_q) = P(M_\infty,s_\infty,s^+_\infty,\mu_\infty,K_\infty,o) \chi \left(\frac{\beta_{r_\infty}}{\beta_r}\right) e^{-i[M_r K - M_{r_\infty} K_\infty]\xi} \qquad (27)$$

The pressure p can then be calculated from (7). It is interesting to note that $(\beta_{r_\infty}/\beta_r)$ which figures in (26) and (27) depends only on the gust characteristics, since

$$\frac{\beta_{r_\infty}}{\beta_r} = \left[1 + \frac{k_3^2}{k_1^2}\right]^{\frac{1}{2}} \quad , \qquad (28)$$

and its value varies significantly for different Fourier components (p,q) of (1).

(b) Reduction to 3-D Gusts in Incompressible Flows for $\theta < 1$.

For $K < K_q$, Eq. (10) is a Klein-Gordon equation similar to that governing the 3-D gust problem in incompressible flow for which $M = 0$. Hence, this class of flows can be reduced to the asymptotic case M=0, by the set of similarity rules:

$$\left.\begin{aligned}
&\text{(i)} \quad M_o = 0 \quad , \\
&\text{(ii)} \quad K_{q_o} = (K_q^2 - K^2)^{\frac{1}{2}} \quad , \\
&\text{(iii)} \quad k_o = k_1/\beta_r^2 \quad , \\
&\text{(iv)} \quad \left(\frac{s_o}{c}\right) = \left(\frac{s}{c}\right)\beta_r \quad , \\
&\text{(v)} \quad \left(\frac{s^+}{c}\right)_o = \left(\frac{s^+}{c}\right) \quad , \\
&\text{(vi)} \quad \cot\mu_o = \beta_r \cot\mu \quad .
\end{aligned}\right\} \qquad (29)$$

Therefore, for the pressure function P we have

$$P(M,s,s^+,\mu,k,K_q) = P(o,s_o,s_o^+,\mu_o,k_o,K_{q_o}) \chi (1/\beta_r) e^{-iM_r K\xi} \qquad (30)$$

For $K = K_q$, the two similarities overlap and the flow is similar to the incompressible two-dimensional case studied by Sears [16].

Because of these similarity rules, it is possible to use the computer codes developed for the asymptotic cases $\theta = \infty$ and $M = o$ to calculate the aerodynamics of the general three-dimensional gust problem. For $\theta = \infty$, we have used a code written by Desmarais at NASA Ames Research Center for a single airfoil and for a cascade Dr. Groeneweg from NASA Lewis Research Center provided us with a code written by Ventres. For M=o, we have modified these codes using Graham mathematical analogy by the complex variable transformation,

$$x \longrightarrow ix$$
$$y \longrightarrow iy \quad .$$

IV. Aerodynamic Results

The jump in the aerodynamic pressure [P] along the blades surface represents a dipole distribution, and therefore directly affects the acoustic radiation. In the following, we briefly discuss the effects of compressibility, and spanwise wave number of the gust, k_3 for a single airfoil and a cascade.

Figure (4) shows plots of the unsteady lift L per unit span acting upon a single flat plate airfoil at $M_o = 0.8$. L is normalized with respect to $(\pi\rho U_r ac)$. The real part of L is plotted in abscissa and the imaginary part in ordinates. Along each curve the value of k_3 is fixed while the reduced frequency is varied from 0 to 5. Comparison with the popular Sears function [16] and Graham's results [15] and [17] shows significant effects due to M_r and k_3. The abrupt change in behavior of constant k_3 curves occurs at $K = K_q$. For $K > K_q$ the flow is similar to a two-dimensional compressible

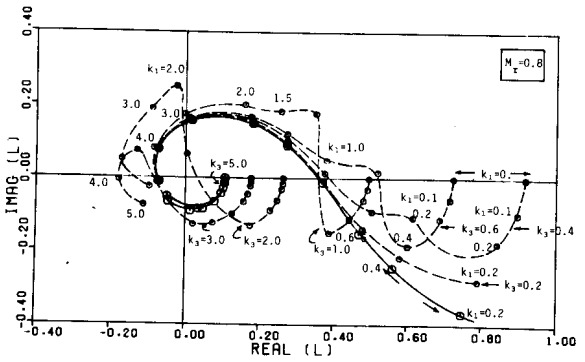

Fig. 4 The Lift Coefficient L for a Single Airfoil for k_3 = 0.0, 0.2, 0.4, 0.6, 1.0, 2.0, and 3.0. The reduced frequency is varied along each curve from 0 to 5.

flow, while for $K < K_0$, the flow is similar to the three-dimensional gust in incompressible flow. For $K = K_0$, we find the classical Sears' results. It is to be noted that though increased Mach number tends to increase the magnitude of L, because of the effect of k_3, increased reduced frequency does not necessarily lead to lower L.

Figure (5) shows a comparison between the unsteady pressure distributions for a single airfoil and a cascade at $M_0 = 0.4$ and $M_0 = 0.8$, both at $k_3=0$ and interblade phase angle $\sigma = \pi/5$. Cascade effects become significant at higher Mach number. Figure (6) shows a similar comparison for $M_0 = 0.8$, and $k_3=1$, and $\sigma = 2$.

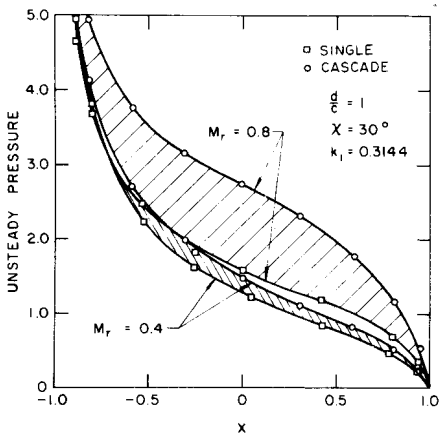

Fig. 5 The Normalized Unsteady Pressure Distribution for a Single Airfoil and a Cascade, k_3 = 0.0.

We note that for the flow conditions of Fig. 6, the lifts for a single airfoil and a cascade are only ten percent apart. However, their pressure distribution shows more significant differences. This will affect accordingly noise calculations taking non-compact source effects into account.

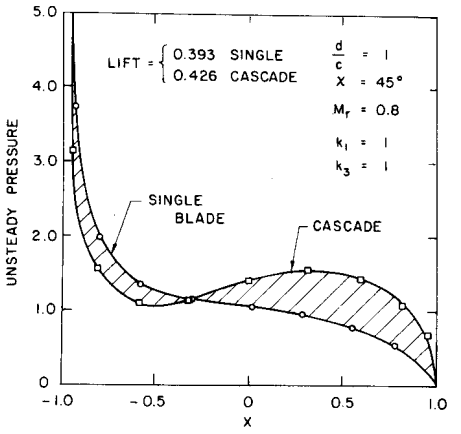

Fig. 6 The Normalized Unsteady Pressure Distribution for a Single Airfoil and a Cascade, k_3 = 1.0.

At resonance conditions the lift of a cascade blade vanishes. This is shown in Figure (7) where the lift coefficients for a single airfoil and a cascade are ploted versus the Mach number for a very large cascade spacing d/c = 10 and $\mu = 50°$. As we approach resonance conditions at M = 0.931, the cascade lift rises above that of a single airfoils then decreases steeply to zero. This essential difference between the two cases is important to consider for acoustic calculations at near resonance conditions.

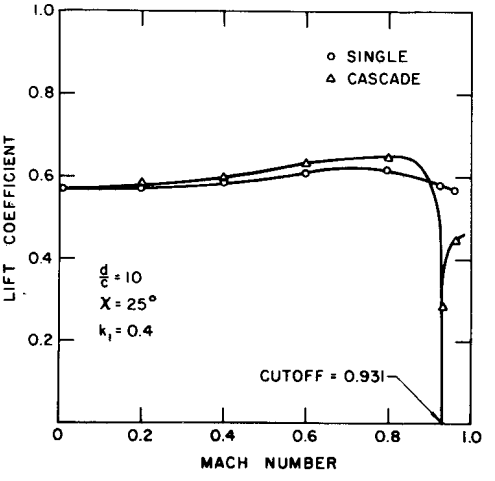

Fig. 7 The Lift Coefficient L for a Single Airfoil and a Cascade Versus M_r.

V. Acoustic Solution

The upstream and downstream radiated acoustic waves are given by the farfield solution of (17) as $\xi \to \mp \infty$, respectively. It is shown in [1] that this acoustic solution corresponds to the real poles of the bracketed term of (17). These poles are given by

$$\alpha_n^{\pm} = -\frac{c s^+}{d^{+2}} \Gamma_n \mp \left[\kappa^2 - \left(\frac{c\Gamma_n}{d^+}\right)^2\right]^{\frac{1}{2}} \quad \text{for } n=0,\pm 1,\pm 2,.. \tag{31}$$

Acoustic waves will exist only if $\alpha_n^{\pm}$ are real, that is

$$\kappa^2 = K^2 - K_q^2 > \left(\frac{c\Gamma_n}{d^+}\right)^2 \qquad (32)$$

Thus the total acoustic solution is a superposition of a number of eigenfunctions which are called modes. Condition (32) marks the boundary between acoustic propagation and exponential decay for any mode. Therefore n has minimum and maximum values of m_1 and m_2, respectively for which inequality (32) holds. Condition (32) will be referred to as the cut-off condition since a mode n will be cut-off if this inequality is not satisfied. The expression for the acoustic pressure is derived in [1] as

$$\left.\begin{aligned} p &\sim \sum_{n=m_1}^{m_2} p_n^+ \quad , \quad \text{as} \quad \xi \to -\infty \\ p &\sim \sum_{n=m_1}^{m_2} p_n^- \quad \text{as} \quad \xi \to +\infty \end{aligned}\right\} \qquad (33)$$

where for each mode n

$$p_n^{\pm} = -(\rho_o a U_r) \frac{\pi c \cos\theta_n^{\pm}}{d^+ \sin\delta_n} f_o(\kappa \sin\theta_n^{\pm}) \qquad (34)$$

$$\chi\, e^{-i[\omega t + (\kappa \sin\theta_n^{\pm} + M_r K)\xi - K(\cos\theta_n^{\pm})\eta]} \cos\left(\frac{\pi q z}{b}\right)$$

with

$$\left.\begin{aligned} \delta_n &= \cos^{-1}\left(\frac{c\Gamma_n}{\kappa d^+}\right) \quad , \\ \theta_n^{\pm} &= -\chi^+ \pm \delta_n \quad , \\ \chi^+ &= \tan^{-1}\left(\frac{s^+}{s\beta_r}\right) \quad . \\ \alpha_n^{\pm} &= \kappa \sin\theta_n^{\pm} \end{aligned}\right\} \qquad (35)$$

These expressions are all derived in terms of the fan parameters. They show how each mode component of the acoustic pressure is generated in terms of the aerodynamics of the fan. Hence in what follows we will first study the conditions of existence and the properties of the acoustic solution in terms of the aerodynamic parameters. But since the sound is radiated outside after crossing the fan duct, we will later study the sound field in terms of the duct parameters.

1. The Cut-Off Condition

Condition (32) determines the number of modes in the acoustic solution for each harmonic (p,q) of disturbance (1), and for given cascade geometry and Mach number M_r. Substituting (25) and (20) for Γ_n, we find that at given M_r and spanwise member k_3, there is a range of reduced frequency k_1 for each mode number n for which inequality (32) is satisfied. Figures 8 and 9 show the ranges of propagating frequencies for spanwise wave numbers

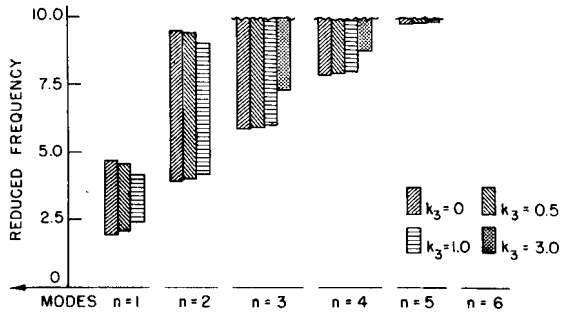

Fig. 8 The Reduced Frequency Range for Propagating Modes for $k_3 = 0.0$, 0.5, 1.0, and 3.0. $M_r = 0.4$.

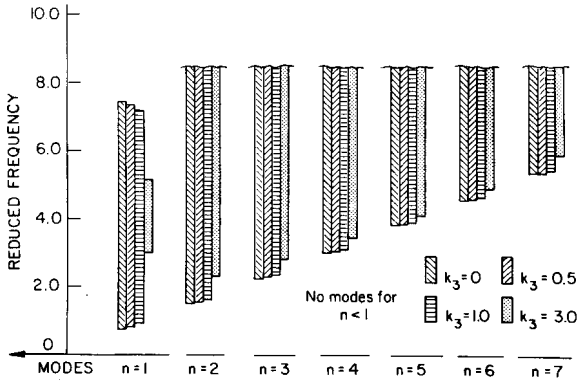

Fig. 9 The Reduced Frequency Range for Propagating Modes for $k_3 = 0.0$, 0.5, 1.0, and 3.0. $M_r = 0.8$.

0.0, 0.5, 1.0, and 3.0, for several acoustic modes at Mach numbers 0.4 and 0.8, respectively; the stagger angle $\chi = 45°$ and $\mu = 67.5$. For each mode the shaded columns show the frequency range at which the acoustic mode will propagate. When the upper limit of k_1 is very high ($k_1 > 10$), the four columns are cut. Hence once a mode appears at a given frequency, only a finite number of its harmonics, if any, will also appear in the solution. For example, in figure 8 we see that for n=1, if the fundamental frequency corresponds to k_1=2.5, none of its harmonics will propagate because the upper limit at which mode n=1 is cut, is below k_1=5. Therefore the upper cut-off limit for k_1 is significant for low mode members n and large k_3. For fixed reduced frequencies, k_1, the ranges of k_3 are shown in Figure 10 for $M_r = 0.8$, and the same cascade parameters as in Figs. 8 and 9. Again we note that there exists an upper limit for q above which no sound will propagate in response to a (p,q) disturbance of (1).

As the reduced frequency is increased more acoustic modes appear in the solution. Hence higher order harmonics contain more propagating modes than lower order harmonics. On the other hand as the Mach number is increased, the lower cut-off frequency is reduced while the upper cut-off limit is increased, thus extending the frequency range for which a mode can exist. This is shown in Figure 11 for a staggered cascade at 45°, μ=67.6°, d/c = 1, and n=1. Three-dimensional effects of the gust are illustrated by the effect of k_3 on the admissible frequency range. As k_3 is increased the

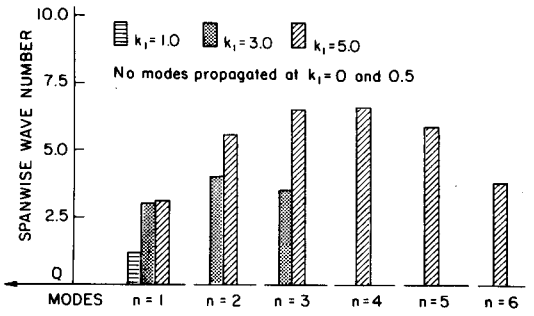

Fig. 10 The k_3-Range for Propagating Modes for $k_1 = 0.0$, 0.5, 1.0, 3.0, and 5.0. $M_r = 0.8$.

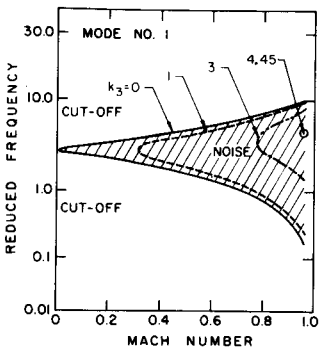

Fig. 11 The Reduced Frequency Range for Mode n=1 Versus M_r at Constant k_3.

k_1-range is reduced. For $k_3 = 4.45$, the k_1-range is reduced to a point and mode n=1 will no more propagate.

2. Non-Compact Source Effects

The present analysis of course accounts for non-compact source effects since it uses a full solution of the unsteady flowfield. However in many other analyses using Lighthill's analogy the compact source approximation is used. This is tantamount to replacing $f_0(\alpha_n^{\pm})$ in (34) by L/2. The relationship between f_0 and the pressure jump along the blade surface is given by

$$f_0(\alpha) = \frac{1}{2\pi} \int_{-\frac{1}{2}}^{\frac{1}{2}} [P] \, e^{i(\alpha + M_r K)\xi} \, d\xi \, . \qquad (36)$$

The lift corresponds to $f_0(\alpha = -M_r K)$. To evaluate the compact-source approximation we have plotted in Figure 12 the function $f_0(\alpha)$ for a single blade at $M_r = 0.8$, $k_1 = 5$ and $k_3 = 0$. Table1 gives the values of $\alpha_n^{\pm}$ for the six modes making up the sound field under these conditions.

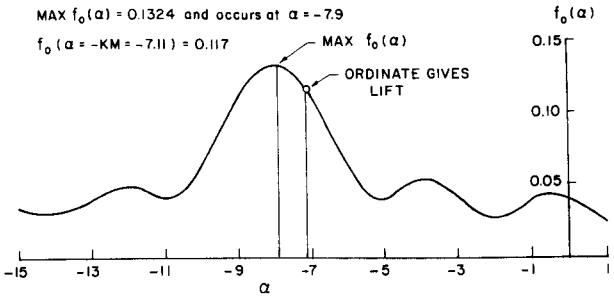

Fig. 12 The Function $f_0(\alpha)$ for a single airfoil at $M_r = 0.8$, $k_1 = 5.0$, and $k_3 = 0.0$.

Mode Number	Upstream	Downstream
n	α_n^+	α_n^-
1	-11.68	-22.17
2	- .82	-19.98
3	7.33	-15.15
4	13.99	- 8.6
5	19.21	- .83
6	22.18	9.25

Table 1. Values of $\alpha_n^{\pm}$ for each mode.

The ordinate giving the value of the lift is $\alpha = -7.11$. Thus we observe that the compact source approximation may overestimate the acoustic pressure by a factor of 2 to 3 for most modes. But because the maximum value of $f_0(\alpha)$ occurs at $\alpha = -7.9$, it is also possible that it may also underestimate the acoustic pressure for some modes.

3. Radiated Acoustic Power

The expression for the radiated acoustic power for the 3-D acoustic waves defined by (32) was derived by Atassi [18] for each mode

$$\frac{W_n^+}{\rho_0 c_0 a^2 S} = \frac{\pi^2}{4} K \kappa \left(\frac{c}{d^+}\right)^2 M_r^2 \beta_r^4 \frac{\cos\chi}{\cos\chi^+} \left| f_0(\kappa \sin\theta_n^{\pm}) \right|^2 \chi \frac{\cos^2 \theta_n^{\pm}}{\sin \delta_n} \times \frac{1}{[K + M_r \kappa \sin\theta_n^{\pm}]} \mathcal{L}, \qquad (37)$$

where S = Bbd, is the cross-sectional area of the duct, and B the number of blades. As mentioned earlier, the compact source approximation consists of replacing f_0 by L/2.

Because the sound pressure level is an important ingredient for the radiated acoustic power, we have plotted its variations for mode n=1, versus k_1 for upstream and downstream waves at k_3=0.2 and 1.0 in Figures 13 and 14, respectively. The other parameters are M_r=0.8, $\chi = 45°$, and $\mu = 67.5°$. We note that the sound pressure rises sharply near cut-off conditions. Indeed, the expression of p_n has $f_0(\alpha)$ in its numerator, and $\sin \delta_n$ in the denominator. Both terms vanish at cut-off conditions. However, an analysis by Atassi [18] shows that the limit of $f_0/\sin\delta_n$ is finite at cut-off. Hence p_n tends to a finite limit for a cascade, but is of course infinite for a single blade. The reason of the sharp rise in P_n near cut-off shown in Figures 13 and 14 is due to inaccurate numerical evaluation of $f_0(\alpha)$ near cut-off conditions. On the other

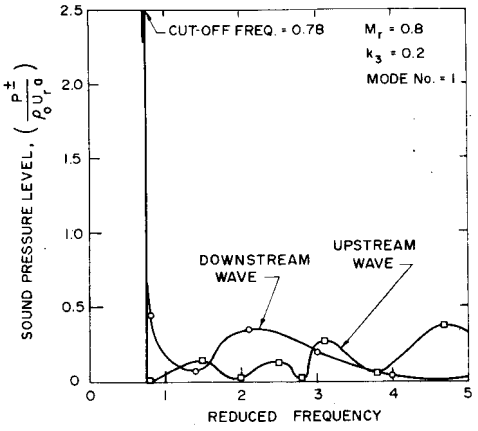

Fig. 13 Sound Pressure Level for Mode n=1, Versus Reduced Frequency for a Cascade. $\chi = 45°$, $d/c=1$, $\mu = 67.5°$, $k_3=0.2$.

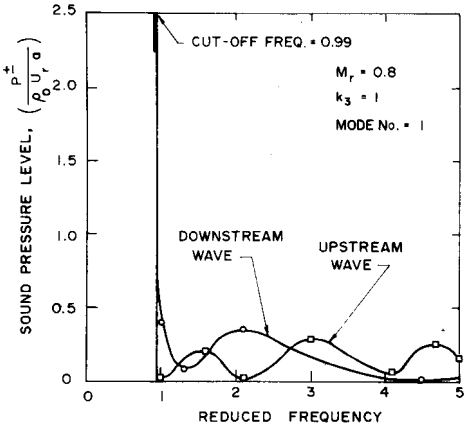

Fig. 14 Sound Pressure Level for Mode n=1, Versus Reduced Frequency for a Cascade. $\chi = 45°$, $d/c = 1$, $\mu = 67.5°$, $k_3 = 1.0$.

hand, W_n should vanish at cut-off conditions for a cascade since its expression contains the square of $f_0(\alpha)$.

The total radiated power for a harmonic component (p,q) of (1) is

$$W^{\pm} = \sum_{n=m_1}^{m_2} W_n^{\pm} \quad . \tag{38}$$

For the same cascade and flow conditions we have plotted in Figures 15 to 18 the normalized acoustic power

$$W^* = W/(\rho_0 \, c_0 \, a^2 \, S) \tag{39}$$

versus the reduced frequency for $k_3 = 0.2$, 0.6, 1.0, 3.0, and 5.0, for upstream and downstream propagating waves. At frequencies corresponding to cut-off conditions a new mode appears in the acoustic solution and modifies the behavior of W^* vs k_1. Therefore in order to get smooth curves one has to calculate a large number or points near cut-off conditions. In order to save on computer time we have limited the number of points in our computations. As a result, the curves of W^* vs k_1 are not smooth.

We notice that at $M_r = 0.8$, the acoustic power is about five times larger for downstream waves than for upstream waves. Besides the peak in the former occurs around $k_1 \sim 2$, while for the latter it is around 3.5. The 3-D effects are quite significant at $k_3 \geq 1$, while they are small at smaller k_3.

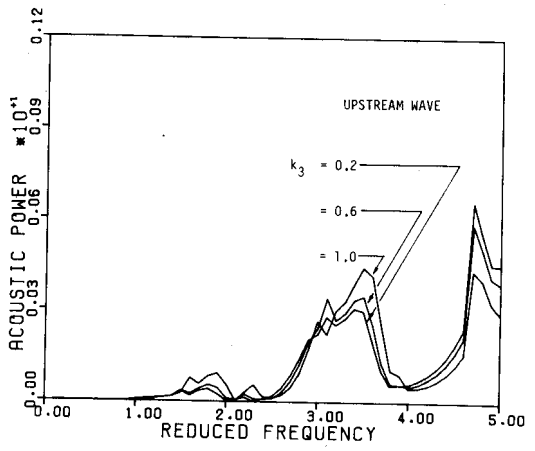

Fig. 15 Acoustic Power Radiated in Upstream Direction. $k_3 = 0.2$, 0.6, 1.0.

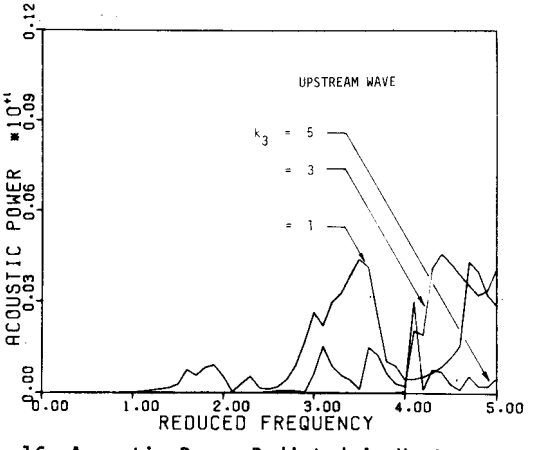

Fig. 16 Acoustic Power Radiated in Upstream Direction. $k_3 = 1.0$, 3.0, 5.0.

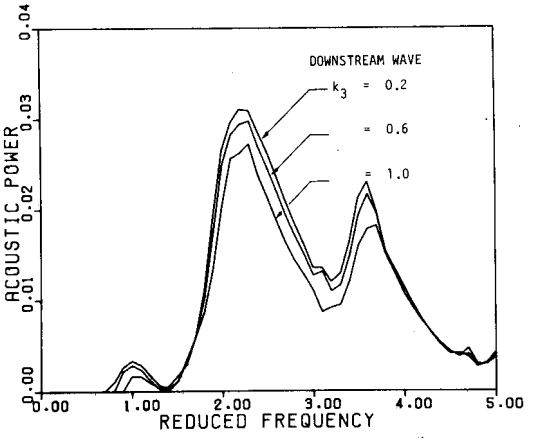

Fig. 17 Acoustic Power Radiation in Downstream $k_3 = 0.2$, 0.6, 1.0.

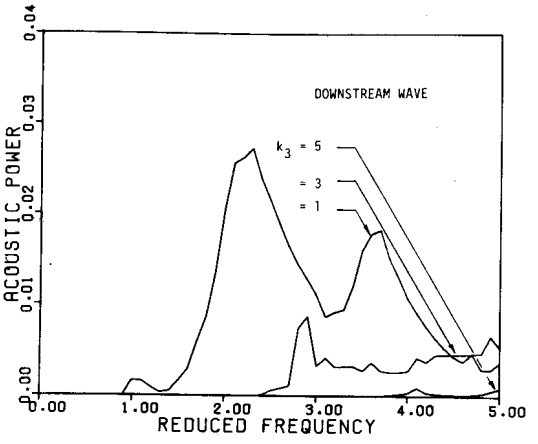

Fig. 18 Acoustic Power Radiation in Downstream Direction $k_3 = 1.0, 3.0, 5.0$.

VI. Noise Generated by Rotor Wake Stator Interaction

We have so far only considered noise produced in a cascade placed in a rectangular duct and subject to a sinusoidal disturbance (p,q). Rotor wake flow irregularities, however, are quite complex but they can be expanded in a double Fourier Series as in (1). The spectrum and power of the noise radiated will then strongly depend on the actual wake velocity profile.

Two typical wake velocity irregularities will be studied. First, we consider a velocity defect due to the viscous wake behind each blade. It will be assumed that this velocity defect extends uniformly along the blade span and hence represents a two-dimensional disturbance. The second type of disturbances considered is that of a tip vortex consisting of swirling flow round the mean flow velocity. Figure 19 shows schematically the two types of

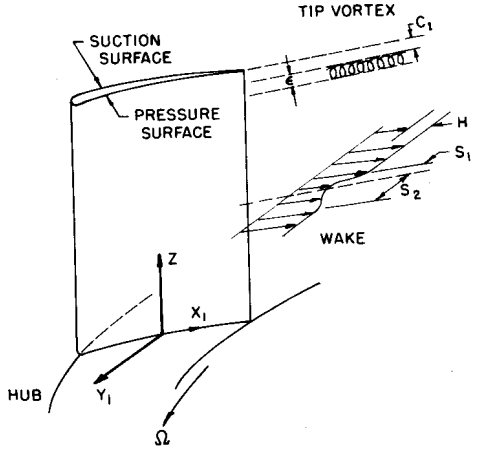

Fig. 19. Schematic of Rotor Wake Velocity Defect and Tip Vortex.

disturbances. All the results discussed below are for $\chi = 45°$, $\mu = 67.5°$, and d/c = 1.

1. Rotor Wake Defect Stator Interaction

Recent measurements reported in [7] and [8] suggest that a two-dimensional model for rotor wake defect would be adequate. This corresponds to $B_{p,q} = o$ in (1) for all q and $A_{p,q} = o$ for all $q \neq o$. Hence, omitting the index q, the upstream flow disturbance can be expanded in a single Fourier expansion

$$\vec{q}_\infty = \sum_p \vec{I}_1 A_p \, e^{i\bar{p}B\Omega[(x_2 + y_2 \cot\mu)/U_r - t]} \qquad (38)$$

Data in [7] and [8] indicate that $\vec{q}_\infty$ can be represented by a triangular profile of height H and base width $(s_1 + s_2)$, alternating at interval $\ell = \lambda \cos\nu$. This profile was used to calculate the noise level of a single loaded blade by Atassi [19] who gives the coefficients of expansion (38)

$$A_p = \frac{H}{4\pi^2 p^2}\left[\frac{(1-e^{-2ip\pi s_1/\ell})}{(s_1/\ell)} - \frac{(1-e^{-2ip\pi s_2/\ell})}{(s_2/\ell)} e^{-2ip\pi s_1/\ell}\right]. \qquad (39)$$

Ravindranath and Lakshminarayana give the following data at blade midspan from the rotor trailing edge

x/c_r	0.01	0.02	0.14	0.35	0.53
H/U_∞	0.82	0.77	0.31	0.24	0.16
$(s_1+s_2)/\ell$	0.08	0.15	0.17	0.18	0.20

Therefore we should expect a considerable influence of rotor-stator axial separation on the noise spectrum and the acoustic power radiated. The total acoustic power radiated is given by

$$W^{\pm} = \sin^2\mu \sum_{p=-\infty}^{p=+\infty} A_p^2 \sum_{n=m_1}^{n=m_2} W^{\pm}_{p,n} \qquad (40)$$

The effects of the wake width are shown in Figure (20) for upstream waves where we have plotted the acoustic power radiated for each harmonic for two symmetric wakes ($s_1 = s_2$) of width 0.17 and 0.20, respectively. The fundamental harmonic corresponds to the blade passing frequency BΩ, where B is the number of rotor blades. Harmonic frequencies are normalized as reduced frequencies $p(B\Omega)c/(2U_r)$. In this figure BPF = $(B\Omega)c/(2U_r)$. In the present case BPF = 1.5.

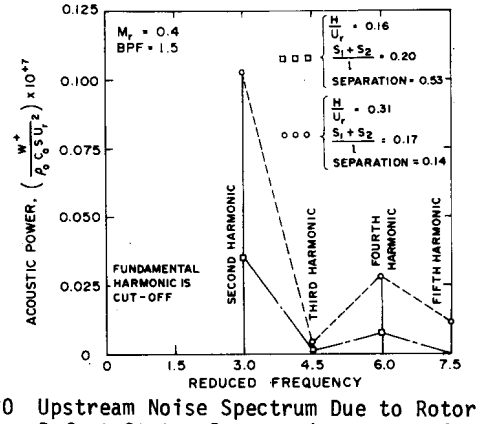

Fig. 20 Upstream Noise Spectrum Due to Rotor Wake Defect Stator Interaction. $M_r = 0.4$.

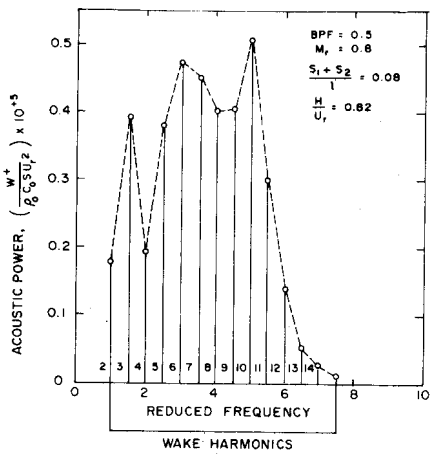

Fig. 21 Upstream Noise Spectrum Due to Rotor Wake Defect-Stator Interaction. M_r = 0.8.

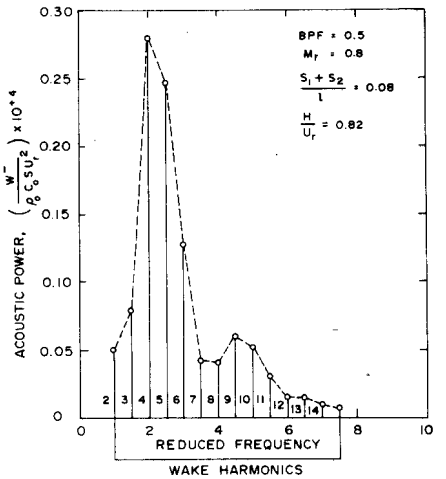

Fig. 22 Downstream Noise Spectrum Due to Rotor Wake Defect-Stator Interaction. M_r = 0.8.

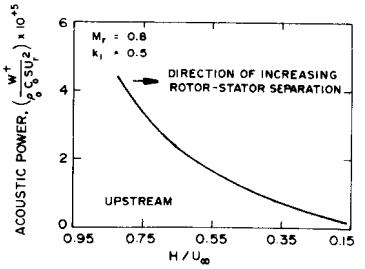

Fig. 23 Upstream Acoustic Power vs Amplitude of Defect Velocity as the Wake Moves Downstream.

We note that the fundamental harmonic is cut-off such at each high BPF. Also it is interesting to note that even a small change of the wake width can produce significant variation in the noise spectrum. Figures (21) and (22) again show the noise spectrum but for higher Mach number (0.8) and at smaller BPF (0.5). We note that for the noise propagating downstream the acoustic power is mainly concentrated in the 4th and 5th harmonics, while it is more evenly distributed between the 3rd to the 10th harmonics for sound propagating upstream.

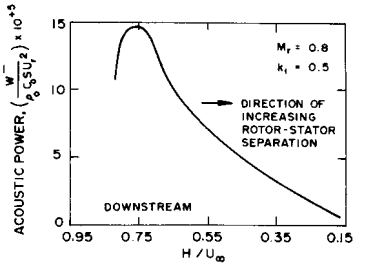

Fig. 24 Downstream Acoustic Power vs Amplitude of Defect Velocity as the Wake Moves Downstream.

In order to illustrate the effect of rotor-stator separation on the total acoustic power, we have used the above data assuming that the stator will not affect the wake characteristics. This is shown in Figures (23) and (24) for upstream and downstream propagating sound, respectively. The acoustic power drops significantly as rotor-stator separation is increased.

2. Rotor Tip-Vortex Stator Interaction

We consider a tip vortex (Fig. 19) of diameter ε and intensity A located at a distance c_ℓ from the upper fan wall. The corresponding upstream disturbance is

$$\vec{q}_\infty = \sum_{p,q} B_{p,q}[\vec{J}_1 \cos(\frac{\pi q z}{b}) - \vec{K} \frac{2ipb}{L_0 q \cos\nu} \sin(\frac{\pi q z}{b})] \times e^{ipB\Omega[(x_2 + y_2 \cot\mu)/U_r - t]} \qquad (41)$$

with $B_{p,q}$ obtained by simple Fourier expansion

$$B_{p,q} = (-1)^{q-1} \frac{4A}{\pi^2} \frac{\sin(\frac{pk\varepsilon}{\lambda\cos\nu})\sin(\frac{\pi q\varepsilon}{2b})\sin(\pi q \frac{2c_\ell + \varepsilon}{2b})}{(\frac{k^2 b q^3}{\pi} + \frac{\pi q^2 P}{b})} \qquad (42)$$

$$B_{o,q} = (-1)^{(q-1)} \frac{2b^2 kA\varepsilon}{\pi^3 q^2 \lambda\cos\nu} \sin(\frac{\pi q\varepsilon}{2b})\sin(\frac{2c_\ell + \varepsilon}{2b})$$

$$B_{p,o} = o, \quad \text{all } p.$$

Smoke visualization pictures of the tip vortex taken by Hansen et al. [20] show that ε is between .05b and 0.10b. Experimental results from [8] indicate that the magnitude of the velocity disturbance H/U_∞ near the vortex boundary is between 0.2 to 0.4. Hence we can relate the vortex intensity to H by Stokes' theorem and we obtain

$$A = \frac{2H}{\varepsilon} \quad . \qquad (43)$$

The total acoustic power is then given by

$$W^{\pm} = \cos^2\mu \sum_{p=-\infty}^{p=+\infty} \sum_{q=1}^{\infty} B_{p,q}^2 \sum_{n=m_1}^{n=m_2} W^{\pm}_{p,q,n} \qquad (44)$$

The cut-off condition and the fast decay of $B_{p,q}$ as p and q increase make it only necessary to calculate a limited number of terms.

Figures 25 and 26 show the noise spectrum

produced by a tip vortex with BPF=0.5, M_r=0.8, $\epsilon/b = 0.05$ for upstream and downstream propagating waves, respectively. The basic spanwise wave number (q=1) is taken here as $k_3 = \pi c/(2b) = 0.2$. We note that downstream radiated noise is dominated by the second harmonic. Experimental results show that the vortex size increases as it moves downstream. Figure 27 and 28 show the effect of increasing ϵ/b on the total acoustic power for the same circulation round the vortex. The acoustic power drops but not as steeply as in the case of wake defect.

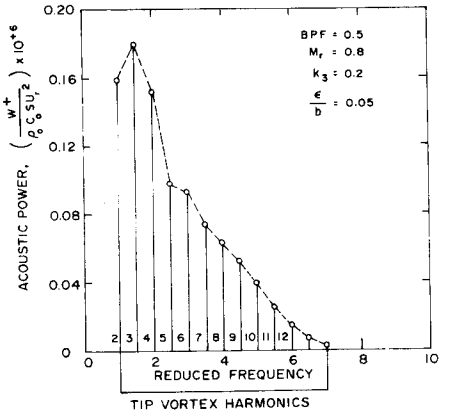

Fig. 25 Upstream Noise Spectrum Due to Rotor Tip Vortex-Stator Interaction.

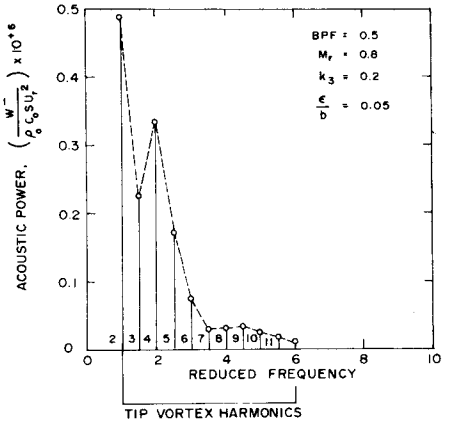

Fig. 26 Downstream Noise Spectrum Due to Rotor Tip Vortex-Stator Interaction.

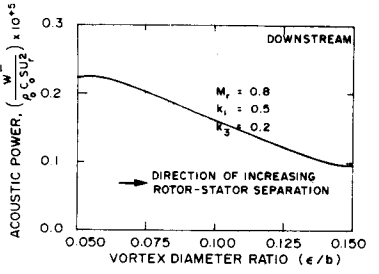

Fig. 27 Downstream Acoustic Power vs Vortex Radius. The Circulation Round the Vortex is Held Constant.

It is important to note that the radiated acoustic power produced by a tip vortex remains much smaller than that generated by velocity wake defect. However, because the present problem depends on a large number of parameters it is not possible yet to

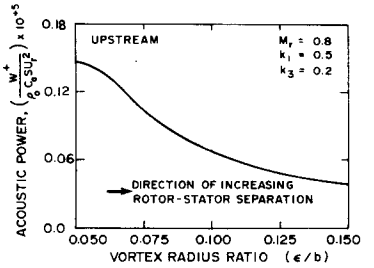

Fig. 28 Upstream Acoustic Power vs Vortex Radius. The circulation round the vortex is held constant.

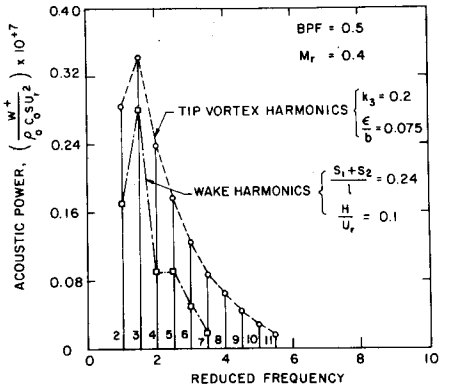

Fig. 29 Upstream Noise Spectrums Due Wake Velocity Defect and Tip Vortex Disturbances.

generalize the present results and to refute the point made by Dittmar about the equal importance of the tip vortex and the wake velocity defect irregularities. In fact, Figure 29 shows a case where the tip vortex generates more upstream noise than the wake velocity defect. More investigations are certainly needed for better understanding of these two noise generating mechanisms.

VI. Concluding Remarks

We have studied discrete tone sound generation in a subsonic fan subject to three-dimensional disturbances. The analytical model used yields directly the radiated sound as the farfield solution of the velocity. The results obtained for each sinusoidal disturbance upstream show significant effects of the spanwise wave number, the cut-off condition, and the non-compactness of the noise sources.

Preliminary results for two typical noise generating flow irregularities were also presented for a rotor wake stator interaction. They indicate that the rotor wake velocity defect produces significantly more radiated acoustic power, particularly downstream, than the rotor tip vortex. This could be attributed to the fact that the wake velocity defect spreads along the full span of the rotor blades, while the tip vortex size was relatively small. Additional investigations using data on wake characteristics will be needed to determine their relative importance.

The results were presented in terms of the aerodynamic parameters of the cascade. This has the advantage of showing how the acoustic field is

generated. Thus we have seen that for every sinusoidal upstream disturbance (p,q), the sound field is composed of a finite number of discrete waves, (modes) each propagating in a different direction. The total sound field for any disturbance will be obtained by summing over all p and q. On the other hand, because the sound is radiated outside after being transmitted through the duct, it is desirable to present the results in terms of the duct parameters. In such a presentation the sound will be considered as the sum of spinning modes. Each spinning mode is the sum of discrete waves but corresponding to different (p,q). The cut-off condition will be accordingly expressed in terms of the mode spinning velocity. Such results will be presented in a later paper.

Acknowledgements

The authors would like to thank Dr. John E. Groeneweg from NASA Lewis Research Center for closely following this work and for his very useful suggestions. They also wish to thank Dr. Marvin E. Goldstein for many helpful discussions.

References

1. Goldstein, M. E., "Aeroacoustics," McGraw-Hill International Book Company, 1976.

2. Tyler, J. M., and Sofrin, T. G., "Axial Flow Compressor Noise Studies," SAE Trans., Vol. 70, 1962, pp. 309-332.

3. Cumpsty, N. A., and Lowrie, B. W., "The Cause of Tone Generation by Aero-Engine Fans at High Subsonic Tip Speeds and the Effect of Forward Speeds," ASME Paper 73-WA/GT-4, Detroit, Mich., 1973.

4. Feiler, C. E. and Merriman, J. E., "Effects of Forward Velocity and Acoustic Treatment on Inlet Fan Noise," AIAA Paper 74-946, Los Angeles, Calif., 1974.

5. Kemp, N. H. and Sears, W. R., "Aerodynamic Interference Between Moving Blade Rows," J. Aeronautical Sci., Vol. 20, No. 9, September 1953, pp. 585-597, and 612.

6. Dittmar, J. H., "Interaction of Rotor Tip Flow Irregularities With Stator Vanes as a Noise Source," NASA TM-73706, 1977.

7. Raj, R. and Lakshminarayana, B., "Three-Dimensional Characteristics of Turbulent Wakes Behind Rotors of Axial Flow Turbomachinery," ASME Journal of Engineering for Power, Vol. 98, April 1976, pp. 218-228.

8. Ravindranath, A. and Lakshminarayana, "Mean Velocity and Decay Characteristics of the Near and Far Wake of a Compressor Rotor Blade of Moderate Loading," J. Eng. Power, Vol. 102, No. 3, July, 1980, pp. 535-548.

9. Lighthill, M. J., "On Sound Generated Aerodynamically: I. General Theory," Proc. Roy. Soc., Series A, Vol. 211, 1952.

10. Goldstein, M. E., Dittmar, J. H. and Gelder, T. F., "Combined Quadrupole-Dipole Model for Inlet Flow Distortion Noise from a Subsonic Fan," NASA TN D-7676, May 1974.

11. Kobayashi, H. and Groeneweg, J. F., "Effects of Inflow Distortion Profiles on Fan Tone Noise," AIAA Journal Vol. 18, No. 8, August 1980, pp. 899-906.

12. Lane, F. and Friedman, M., "Theoretical Investigation of Subsonic Oscillatory Blade-Row Aerodynamics," NACA TN-4136, Feb. 1958.

13. Kaj. S. and Okazaki, T., "Generation of Sound by Rotor-Stator Interaction," Jour. of Sound and Vibration, vol. 13, no. 3, pp. 281-307, 1970.

14. Whitehead, D. S., "Vibration and Sound Generation in a Cascade of Flat Plates in Subsonic Flows," A.R.C., R&M 3685, 1972.

15. Graham, J. M. R., "Similarity Rules for Thin Aerofoils in Non-Stationary Subsonic Flows," Journal of Fluid Mechanics, (1970), vol. 43, Part 4, pp. 753-766.

16. Sears, W. R., "Some Aspects of Nonstationary Airfoil Theory and Its Practical Applications," Journ. of Aeronautical Sciences, vol. 8, no. 3, 1941, pp. 104-108.

17. Graham, J. M. R., "Lifting Surface Theory for the Problem of an Arbitrarily Yawed Sinusoidal Gust Incident on a Thin Airfoil in Incompressible Flow," Aeronautical Quarterly, vol. XXI, part 2, p. 182, May 1972.

18. Atassi, H., "Note on the Acoustic Power Radiated in a Cascade of Airfoils Subject to 3-D Disturbances," University of Notre Dame Report No. 181.

19. Atassi, H., "Effect of Loading and Rotor Wake Characteristics on the Acoustic Field of Stator Blades," AIAA Paper No. 76-566, Palo Alto, Calif., July 1976.

20. Hansen, G., Herzig, H. Z., and Costello, G. R., "A Visualization Study of Secondary Flows in Cascades," NACA TN-2947, May 1953.